NASA/TM–2015-218987

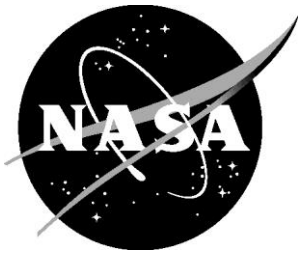

Crash Tests of Three Cessna 172 Aircraft at NASA Langley Research Center's Landing and Impact Research Facility

Justin D. Littell
Langley Research Center, Hampton, Virginia

November 2015

NASA STI Program . . . in Profile

Since its founding, NASA has been dedicated to the advancement of aeronautics and space science. The NASA scientific and technical information (STI) program plays a key part in helping NASA maintain this important role.

The NASA STI program operates under the auspices of the Agency Chief Information Officer. It collects, organizes, provides for archiving, and disseminates NASA's STI. The NASA STI program provides access to the NTRS Registered and its public interface, the NASA Technical Reports Server, thus providing one of the largest collections of aeronautical and space science STI in the world. Results are published in both non-NASA channels and by NASA in the NASA STI Report Series, which includes the following report types:

- TECHNICAL PUBLICATION. Reports of completed research or a major significant phase of research that present the results of NASA Programs and include extensive data or theoretical analysis. Includes compilations of significant scientific and technical data and information deemed to be of continuing reference value. NASA counter-part of peer-reviewed formal professional papers but has less stringent limitations on manuscript length and extent of graphic presentations.

- TECHNICAL MEMORANDUM. Scientific and technical findings that are preliminary or of specialized interest, e.g., quick release reports, working papers, and bibliographies that contain minimal annotation. Does not contain extensive analysis.

- CONTRACTOR REPORT. Scientific and technical findings by NASA-sponsored contractors and grantees.

- CONFERENCE PUBLICATION. Collected papers from scientific and technical conferences, symposia, seminars, or other meetings sponsored or co-sponsored by NASA.

- SPECIAL PUBLICATION. Scientific, technical, or historical information from NASA programs, projects, and missions, often concerned with subjects having substantial public interest.

- TECHNICAL TRANSLATION. English-language translations of foreign scientific and technical material pertinent to NASA's mission.

Specialized services also include organizing and publishing research results, distributing specialized research announcements and feeds, providing information desk and personal search support, and enabling data exchange services.

For more information about the NASA STI program, see the following:

- Access the NASA STI program home page at http://www.sti.nasa.gov

- E-mail your question to help@sti.nasa.gov

- Phone the NASA STI Information Desk at 757-864-9658

- Write to:
  NASA STI Information Desk
  Mail Stop 148
  NASA Langley Research Center
  Hampton, VA 23681-2199

NASA/TM–2015-218987

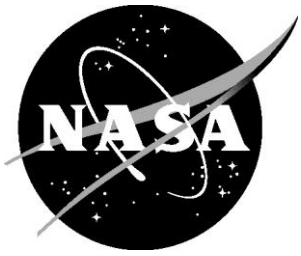

Crash Tests of Three Cessna 172 Aircraft at NASA Langley Research Center's Landing and Impact Research Facility

Justin D. Littell
Langley Research Center, Hampton, Virginia

National Aeronautics and
Space Administration

Langley Research Center
Hampton, Virginia 23681-2199

November 2015

Available from:

NASA STI Program / Mail Stop 148
NASA Langley Research Center
Hampton, VA 23681-2199
Fax: 757-864-6500

Abstract

During the summer of 2015, three Cessna 172 aircraft were crash tested at the Landing and Impact Research Facility (LandIR) at NASA Langley Research Center (LaRC). The three tests simulated three different crash scenarios. The first simulated a flare-to-stall emergency or hard landing onto a rigid surface such as a highway, the second simulated a controlled flight into terrain with a nose down pitch on the aircraft, and the third simulated a controlled flight into terrain with an attempt to unsuccessfully recover the aircraft immediately prior to impact, resulting in a tail strike condition. An on-board data acquisition system captured 64 channels of airframe acceleration, along with acceleration and load in two onboard Hybrid II 50th percentile Anthropomorphic Test Devices, representing the pilot and co-pilot. Each test contained different airframe loading conditions and results show large differences in airframe performance. This paper presents test methods used to conduct the crash tests and will summarize the airframe results from the test series.

Introduction

NASA Langley Research Center's (LaRC) Landing and Impact Research Facility (LandIR), shown in Figure 1, is 240-ft high, 400-ft long steel A-frame gantry structure built in 1965, and originally used to train the Apollo astronauts to land on the moon.

Figure 1 - Landing and Impact Research Facility (LandIR)

After the Apollo program ended in the early 1970s, the LandIR facility was converted into a full-scale aircraft crash facility, and, since the mid-1970s, has been used to test all types of aircraft for the improvement of safety features [1]. General Aviation (GA) airplane testing at LandIR has played a major role in the advancement of safety features amongst GA aircraft including improved aircraft seat test methods and design [2], energy absorbing subfloor concepts for attenuating loading into onboard occupants [3], and Emergency Locator Transmitter (ELT) performance improvements [4]. In addition, a large amount of crash test data was generated originating from a test program initiated in 1972 between NASA and the Federal Aviation Administration (FAA). This test program investigated ways to develop technology for improved crashworthiness in GA airplanes [5]. Multiple series of crash tests were conducted both on low wing [6-9] and high wing [10] aircraft for the investigation of both aircraft performance and occupant survivability. Since the mid-2000s, the LandIR facility has also been used to characterize NASA Orion spacecraft under various land and water landing conditions [11], and, in 2011, the Hydro Impact Basin [12] was built at the west end of the LandIR facility for use in full scale crash and impact testing into water.

The LandIR facility is able to lift and swing various aircraft using a single (which introduces a pitch rate) or parallel (which removes the pitch rate) swing cabling system. Either a single set or a parallel set of swing cables connected to the west end of the LandIR facility attach at hard-points into the aircraft. Pull-back cabling connected to a movable overhead bridge located on the eastern side of the LandIR facility attach to the pullback points of the test article. As the pullback cabling is retracted into the bridge winch system, the

aircraft is lifted into the air to a pre-determined drop height. At the pre-determined height, a pyrotechnic system severs the pullback cabling, causing the test article to swing along a pendulum-like flight path from east to west into a pre-determined impact location on the ground. Immediately before ground contact, an onboard pyrotechnic system severs the single or parallel swing cabling, allowing the aircraft to achieve a pure free fall flight condition during the last few milliseconds of the swing. Various combinations of swing cable length, impact location, drop height, impact surface conditions (rigid, soil or water) along with a test article's angle of attack can be prescribed, creating a large variety of impact conditions.

The test series conducted in the summer of 2015 served to generate data for use in updating the performance specifications for the next generation of ELT systems. ELT systems are present on all GA aircraft and are intended for use in a distress situation, such as an emergency or crash landing of an aircraft. The ELT system is designed to automatically sense a crash event and transmit a distress signal to the Cosmicheskaya Sistyema Poiska Avariynich Sudov – Search and Rescue Satellite Aided Tracking (COSPAS-SARSAT) system. The signal is then relayed down to a ground Local User Terminal (LUT), and ultimately Search and Rescue operatives are dispatched to the aircraft in distress.

Since ELT systems must be designed to work in a potentially infinite number of different scenarios, a sample of three differing impact conditions capable of being replicated at the LandIR facility were selected. It is from the evaluation of these three crash tests that a large range of crash test data were generated.

Airplane Overview

Three Cessna high wing, four seat, GA 172 airplanes were purchased specifically for the test series. They are pictured in Figure 2.

Test article 1 Test article 2 Test article 3

Figure 2 - Airplane test articles

Test article one was a 1958 172 which was current on its annual inspection. Test article two was a 1958 175, which is the 172 airframe, but contains a different engine and gearbox. The third test article was a 1974 172M also current on its annual inspection. Test articles 1 and 3 were flying as late as the winter of 2014, before being transported to NASA LaRC.

Airplane Preparations

Guidance was obtained from previous high-wing aircraft tests conducted in the late-1970's for rigging, lifting and swinging the airplanes [13] at the LandIR facility. Hardware fabricated for this test series was ultimately based on these heritage designs, but included updates and additions due to upgrades in the LandIR facility and data collection systems added since the 1970s.

A single over-wing swing location was chosen as the main swing point to be used in the tests. By selecting a single over wing swing point, a pitch rate is introduced into each airframe, which is a way to simulate a pilot attempting to flare or pull the nose up immediately before impact.

The LandIR main swing cables were attached into each aircraft using hardware designed to interface with the main wing-fuselage attachment points for the main over-wing swing location. For each airplane, the wings were removed and two steel posts were retrofit around the front and rear wing-fuselage attachment points. Aluminum C-channel beams were fastened back-to-back on either side of the steel posts, with a large portion of the channels extending forward of the forward post position. A steel block with swivel hoist ring used as the swing cable attachment point was eventually installed between the C-channel beams, positioned at a distance forward of the forward wing attachment. Because the eventual location of the main swing cables depended on the final center of gravity (CG) location of the airplane, the impact station under the LandIR facility and the pitch angle, this attachment was not installed until after each aircraft was fully ballasted and precise impact conditions were known. Figure 3 shows the over wing attachment hardware, with main swing cable attachment location identified.

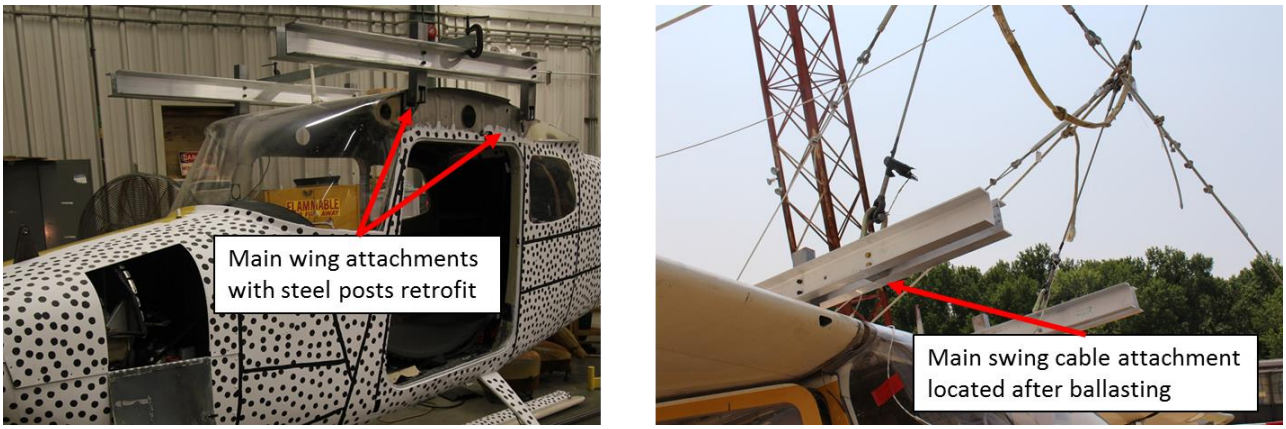

Figure 3 - Main over-wing swing attachment hardware

The main over-wing swing cables attached to the swivel hoist ring on the C-channel and terminated at a pear ring. From the opposite end of the pear ring the main LandIR swing cables were attached. Additional cabling was also attached to the pear ring, which was designed to keep the airplane from losing orientation during the swing. This hardware and cabling was known as the pitch restraint hardware.

The airplane was restricted to its desired impact orientation due to cabling extending from the pear rings to locations forward and aft of the main swing cables. The forward restraint cables attached to hardware retrofit onto the engine, while the rear restraint cables attached to hardware retrofit onto a location near station 108, which is the aft cabin/forward tail junction on the airplane. For each test, once the main swing cables were attached to the airplane, the correct pitch orientation was achieved by adjusting the restraint cable lengths. Figure 4 shows the front pitch restraint hardware.

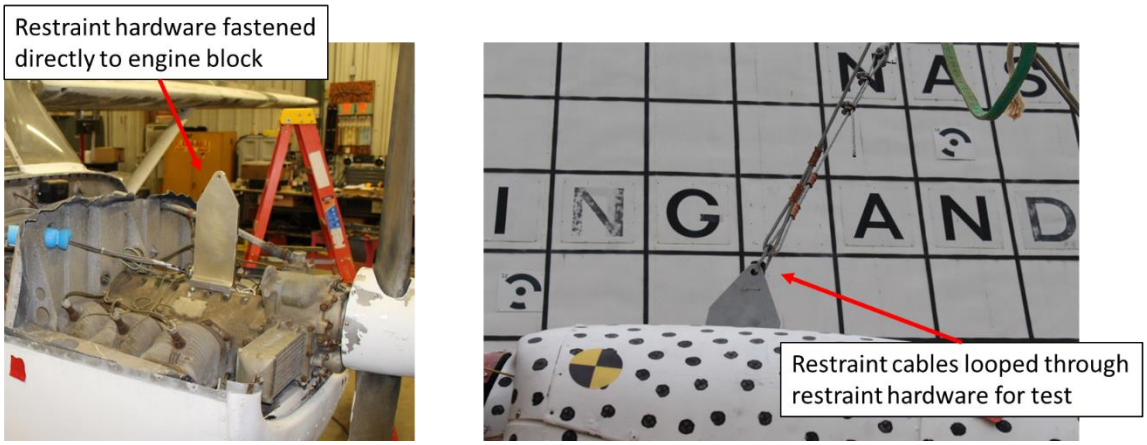

Figure 4 - Front pitch restraint hardware detail

The year and model differences of the airplanes did not adversely affect the design of the front pitch restraint hardware, which was a simple bracket machined from stock material. Since each piece was custom made for each airplane, each engine hole-pattern and the height were pre-programmed into the cutting machine and the stock material was cut to size. The year and model differences did, however, affect the rear pitch restraint hardware design. Airplanes 1 and 2 were an earlier "straight tail" variant of the 172 design. The straight tail design contained a continuous sloping geometry starting at the aft fuselage and terminating at the vertical stabilizer in the rear tail. The straight tail design also included an internal frame stiffener at aircraft station 108. Airplane 3 featured a newer "swept tail" variant of the 172 design. The swept tail included improvements to pilot visibility by adding a rear split window, but removed the frame section at station 108.

In order to facilitate the rear restraint lines on the different designs, two versions of the rear pitch restraint hardware were fabricated. In the straight tail design, the rear pitch restraint hardware was retrofit to the station 108 stiffener, with only an open hole protruding through the exterior of the aircraft skin in which to loop the restraint lines.

In the swept tail design, a doubler-plate was added to the outer skin of the aircraft and attached to stiffening hardware on the interior of the tail. Figure 5 shows both variants of the rear pitch restraint hardware.

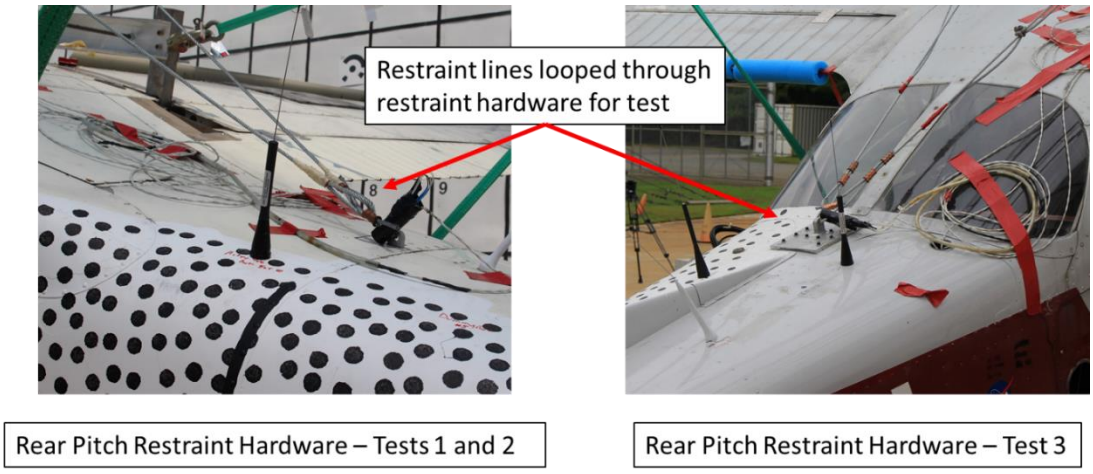

Figure 5 - Rear pitch restraint hardware detail

To facilitate the pullback for each test, each airplane was also outfitted with pullback hardware. The airplane interfaced with the LandIR main pullback cable and spreader bar (used to divide the pullback load evenly to both the north and south sides of the test article) via the pullback hardware. The pullback hardware consisted of two green polyester 1-in. wide straps attached to each side of the airplane. The aft end of the over-wing C-channel swing hardware was also used for the upper pullback strap attachment point, and the lower pullback strap was attached to hardware retrofit onto the landing gear. The straps were fabricated to custom lengths for each aircraft such that the angle created by the projection of the pullback cabling created a right angle with the projected location from the main over-wing swing cables when the airplane was at the correct drop height and orientation. The cable lengths were also designed such that the point of intersection of these two projections was the location of the airplane CG. Figure 6 shows the final test configuration of the airplane/LandIR facility rigging, with the projections of the cabling highlighted.

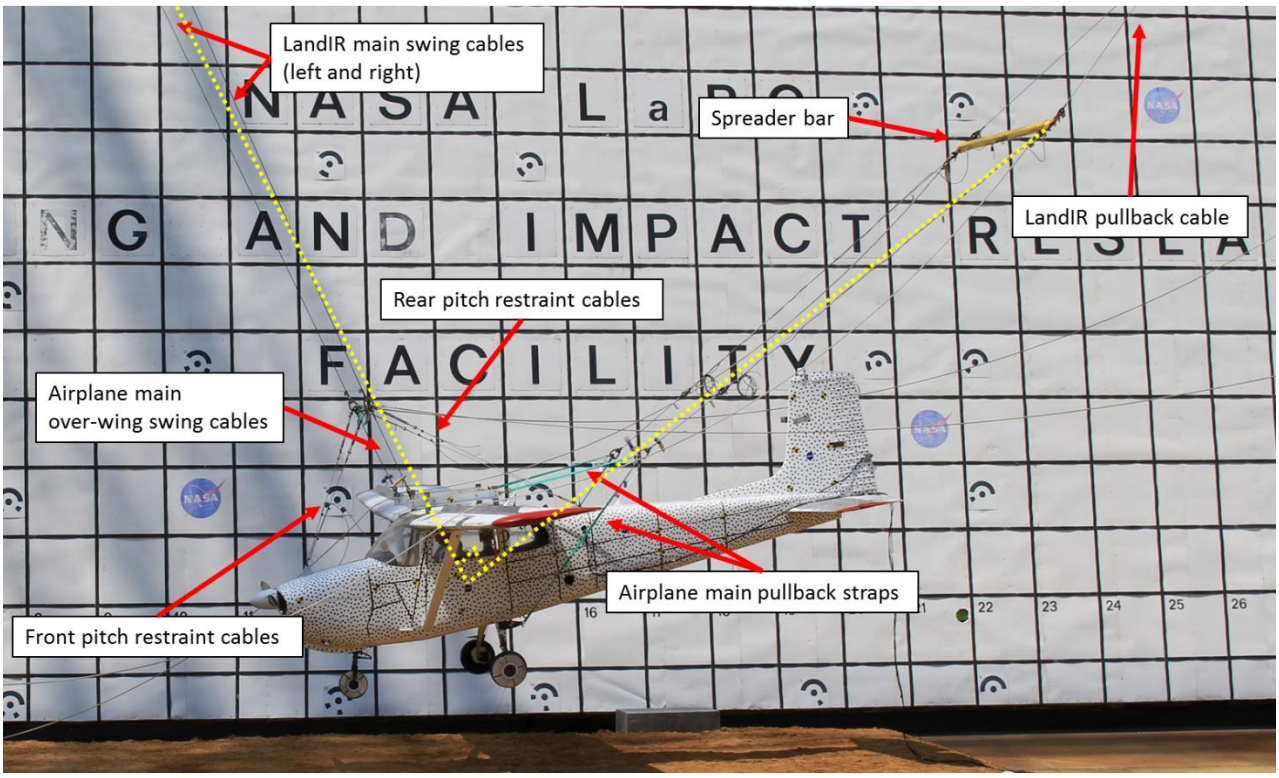

Figure 6 - Airplane rigging in test configuration (Test 2 shown)

Airplane Instrumentation

Each aircraft was prepped with similar instrumentation, cameras and onboard experiments. The rear seats and luggage area equipment were removed from each airplane, and an onboard ruggedized Data Acquisition System (DAS) was installed in its place. This DAS, along with a time-code generator used in data synchronization, and the pyrotechnic cutter firing system were all enclosed in a protective cage, as to keep the systems intact in the event of a large amount of aircraft deformation and/or crushing. The DAS equipment with cage also acted as rear seat/luggage area ballast. Acceleration data were collected from accelerometers located throughout the fuselage along with accelerations and loads from two onboard Anthropomorphic Test Devices (ATDs, a.k.a. crash test dummies). Three ruggedized onboard high speed cameras were also utilized during each test. Additional high-definition cameras filming at either 30 or 60 frames per second were utilized on certain exterior parts of each airplane.

Table 1 shows the channels of airframe acceleration instrumentation, and Table 2 shows ATD instrumentation. All channels were sampled at 10 kHz. The DAS and onboard high speed cameras were connected to computers in the LandIR control room via CAT 5e umbilical cables, and triggered using either a command from the control room computers or a switch button.

Table 1- Airframe instrumentation

Location	Direction
Engine	Horizontal, Vertical, Lateral
Firewall	Horizontal, Vertical
Floor under pilot seat (Pilot Floor)	Horizontal, Vertical
Floor under co-pilot seat (Co-Pilot Floor)	Horizontal, Vertical
Cabin ceiling at aft wing stiffener	Horizontal, Vertical
Left door frame	Horizontal, Vertical
Right door frame	Horizontal, Vertical, Lateral
DAS Rack (Rear Cabin/Luggage area)	Horizontal, Vertical
Tail	Horizontal, Vertical, Lateral

Table 2 - ATD instrumentation

ATD Location	Measurement	Direction
Head	Acceleration	Horizontal, Vertical
Chest	Acceleration	Horizontal
Pelvis	Acceleration	Horizontal, Vertical
Lumbar	Force	Vertical
Seatbelt	Force	Strap tension

Instrumentation installed in the airframe presented in this report is oriented in the local airframe coordinate system, with vertical accelerations being in the Lift/Weight direction, with positive being upward, and horizontal accelerations being in the Thrust/Drag direction, with positive being forward. All accelerations are filtered in accordance to SAE-J211 standards [14].

Other preparations included painting the pilot side of each airplane with a stochastic black and white speckle pattern. This pattern aided with the collection of airframe deformation data from a technique called full field photogrammetry [15]. Solid black lines were painted over the main rivet lines on the skin to aid in tracking of main frame and stiffener locations from the external cameras. Additional lead weight was added over the wing to simulate fuel weight. The lead, along with the main swing hardware, accounted for approximately 100 lb of weight over each wing, which simulated fuel tanks above 75% full. Spoilers were attached to each wing to minimize lift generated due to the swinging of the aircraft during the test. All control surfaces were locked in the VS1 (minimum steady flight speed) configuration, and the yokes were locked in their forward-most position. Finally, multiple ELTs were mounted into the cabin or tail section of each aircraft for the evaluation of their performance.

After all preparations were completed, a weight and balance test was performed on each test article, and is summarized in Table 3. The horizontal CG is measured from the firewall, the lateral CG is measured from the aircraft centerline, and the vertical CG is measured from the ground. The column labeled “Moment / 1000” is calculated by multiplying the weight and horizontal CG. It is this number that is typically found in a Pilot Operating Handbook to determine the aircraft category.

Table 3 - Aircraft test article weight and CG properties

Test	Weight (lb)	Horizontal CG (in.)	Lateral CG (in.)	Vertical CG (in.)	Moment / 1000 (in.-lb)	Category
1	2000	44.5	0.0	46.25	89	Normal
2	2114	39.5	0.0	48.1	101	Normal
3	2072	42.5	0.0	50.8	89	Normal

Crash Test 1 was designed to simulate a flare-to-stall onto a rigid surface such as concrete or road, whereas Tests 2 and 3 were designed to simulate a controlled flight into terrain condition. In Test 2, the airplane impacted soil in a nose down configuration, in contrast to Test 3, where the airplane impacted soil in a nose up, tail strike condition. All tests were conducted in the approximate range of the stall speed of each aircraft.

Table 4 summarizes the as-measured impact conditions for each of the full-scale crash tests.

Table 4 – Measured CG impact conditions

Test	Surface	Horizontal Velocity – ft/sec – fps (kts)	Vertical Velocity – fps (kts)	Flight path velocity – fps (kts)	Angle of Attack (deg)	Pitch Rate (deg/sec)
1	Concrete/Rigid	60.2 (35.7)	23 (13.6)	64.4 (38.2)	+1.5	+16.5
2	GUS	68.6 (40.6)	28.7 (17.0)	74.4 (44.0)	-12.2	+16.1
3	GUS	56.9 (33.7)	23.6 (14.0)	61.6 (36.5)	+8.0	+13.3

The soil surface used in Tests 2 and 3 consisted of a two foot thick bed of a clay-sand mixture, and was known as Gantry Unwashed Sand (GUS) [16]. Soil was characterized for Tests 2 and 3 using three major methods - calculating density, measuring moisture content, and measuring the bearing ratio as a function of depth. These three parameters are likely to determine whether the soil is “hard” or “soft” and whether it is compact (like clay) or silty (like sand). The parameters were measured immediately post-test at a variety of locations around the impact spot. Ranges from the sets of measured parameters are reported, and a graph of the bearing ratio vs. depth is provided in the Test 2 and Test 3 sections.

For all tests, a large yellow catch net was installed on the western side of the impact location to catch and stop the airplane in the event of a large amount of residual horizontal velocity after the impact. The net was intended to restrict the airplane from rolling and plunging into the Hydro Impact Basin approximately 100 feet away from the impact site. The net was designed to break away from its supporting posts upon airplane contact, wrap around and dissipate the airplane motion through the pulling of two large drag weights.

Test 1

Test 1 was conducted on July 1, 2015. Figure 7, left, shows the airplane on the ground prior to the start of pullback, and, right, at the drop height.

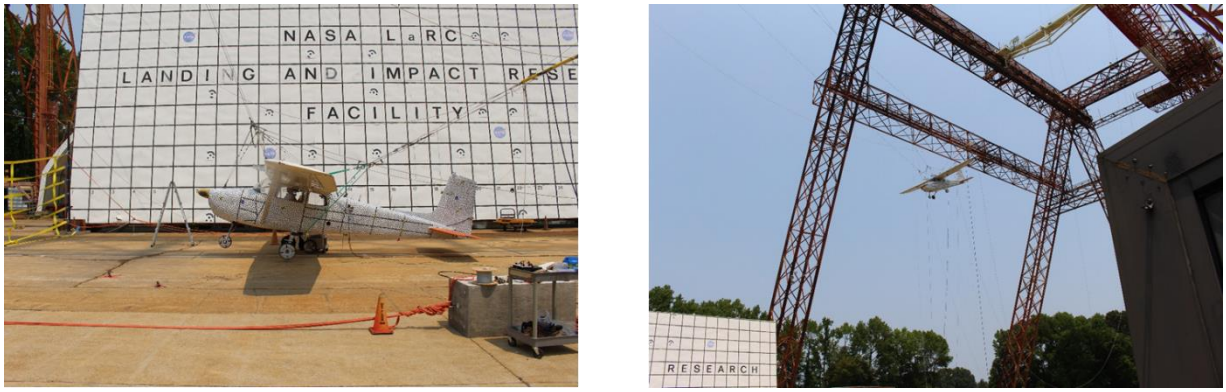

Figure 7 - Airplane configuration prior to Test 1. Airplane on ground (left) and at drop height (right)

In Test 1, the airplane impacted the concrete at a flight path velocity 64.4 ft/sec at an Angle of Attack (AoA) of approximately 1.5° nose high. There was approximately 0.475 sec of time between the initial impact with the ground and the first contact of the catch net. The pitch rotation and large mian gear flexing caused the rear portion of the tail to strike the ground approximately 0.125 sec after impact. The primary vertical ground loading was complete at 0.200 sec, after which the aircraft rebounded with residual horizontal velocity and proceeded to impact the catch net. The propeller first contacted the net approximately 0.475 sec after initial impact. The contact continued stretching the net, until it unlatched from the uprights starting approximately 0.500 sec after initial ground impact. The net continued to wrap around the airplane until it started to move the drag weights approximately 1.120 sec after impact. All motion stopped approximately 5.85 sec after impact. Figure 8 shows the sequence of the ground contact, while Figure 9 shows the sequence of events for the net contact. Table 5 summarizes these events in tabular form.

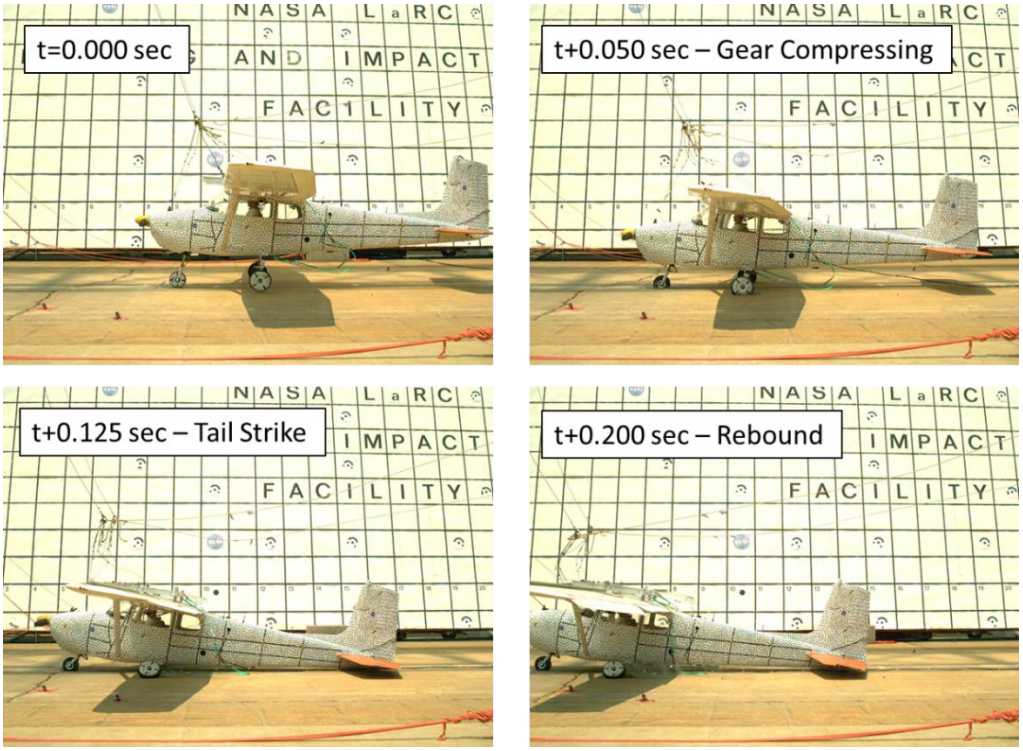

Figure 8 - Test 1 impact sequence – ground contact

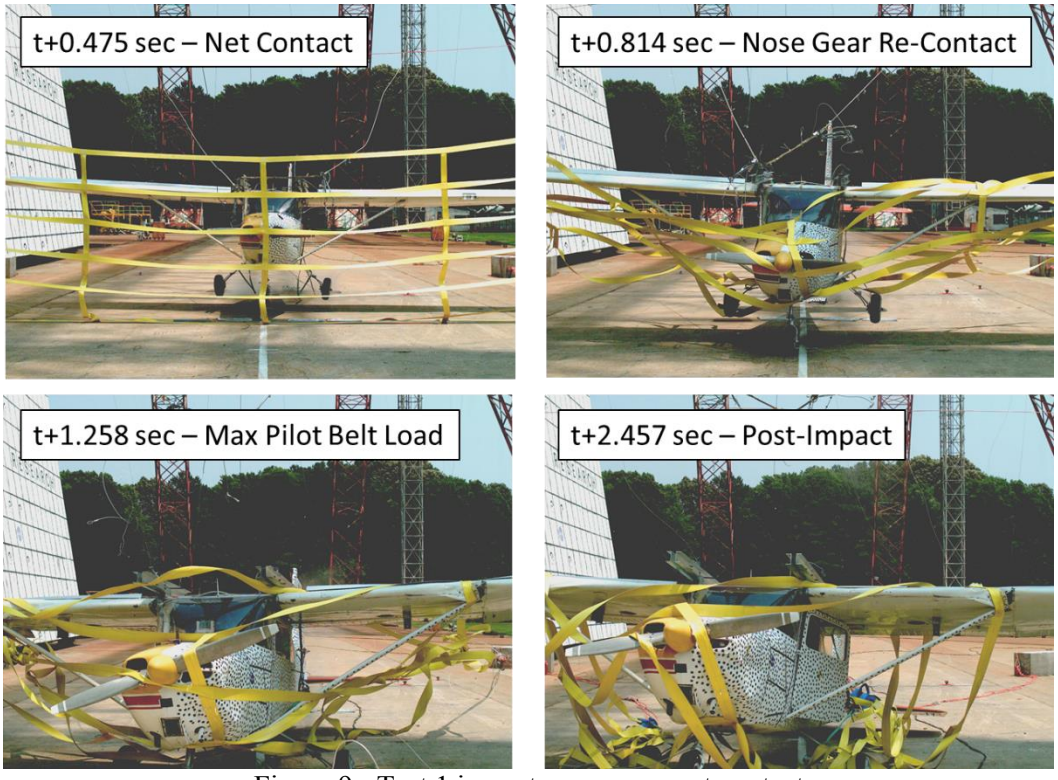

Figure 9 - Test 1 impact sequence - net contact

Table 5 - Event timing for Test 1

Event	Time after impact (sec)
Nose gear impact	0.000
Main gear impact	0.006
Tail strike	0.125
Catch net contact	0.475
Second nose gear impact	0.814
Second main gear impact	0.939
Pilot door open	2.003
Motion Stop	5.835

At a high level, the test can be discussed in terms of two distinct impact events. The first event is the airplane impacting the concrete surface simulating a crash or emergency landing. In this event, which occurs for the first 0.300 sec, the landing gear deforms and the plane rebounds with minimal loss in its original horizontal velocity. As shown in Figure 10, the vertical acceleration shows a roughly trapezoidal shaped pulse resulting from the landing gear deflecting. Examining the plateau in acceleration occurring between 0.015 sec (start of plateau) and 0.200 sec (start of airplane rebound) after impact, the average sustained acceleration varies between 4.1 g in the engine to 5.9 g in the tail. The large 54.7 g peak in the tail is due to the tail strike, which occurred at 0.125 sec after the impact. The horizontal acceleration is minimal with the exception of the noise seen in the tail accelerometer, which is due to the tail strike.

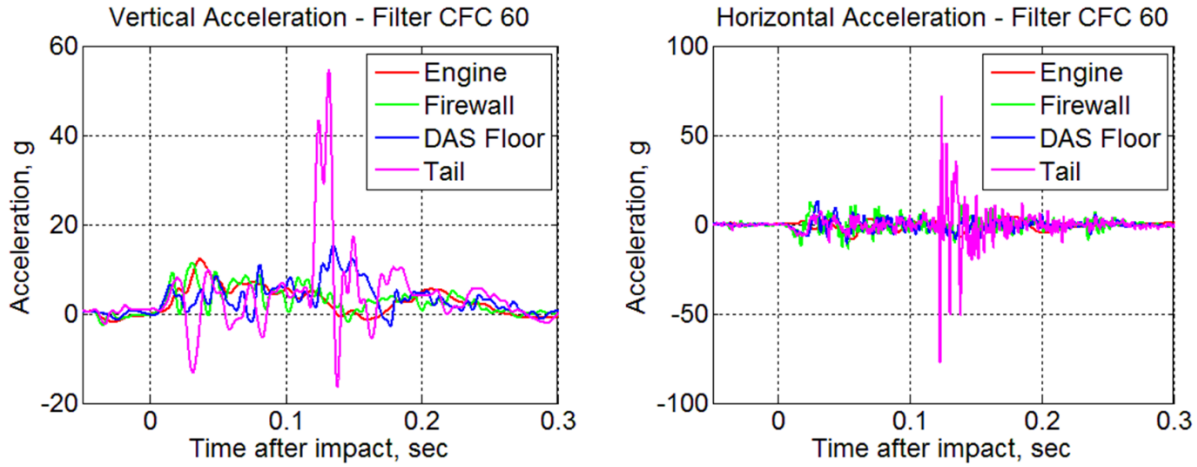

Figure 10 – Test 1 airframe accelerations during ground impact

The second event is the airplane interacting with the catch net. The net was necessary to the test due to the constraints of the LandIR facility and not originally thought to be a part of the test. However, when investigating the results, the net can simulate a real scenario such as an airplane impacting brush, berm or other obstruction after the initial emergency/crash landing. Thus, it should be included in the data analysis in terms of its effect on the loading on the airframe and occupants. As shown in Figure 11, the horizontal acceleration in the airplane resulting from the catch net was a triangular pulse shape, lasting 0.5-sec and reaching average peak accelerations ranging between 4.0 g in the tail to 5.3 g on the engine. The large spike at the end of the net contact in the tail data is a second tail strike onto the concrete.

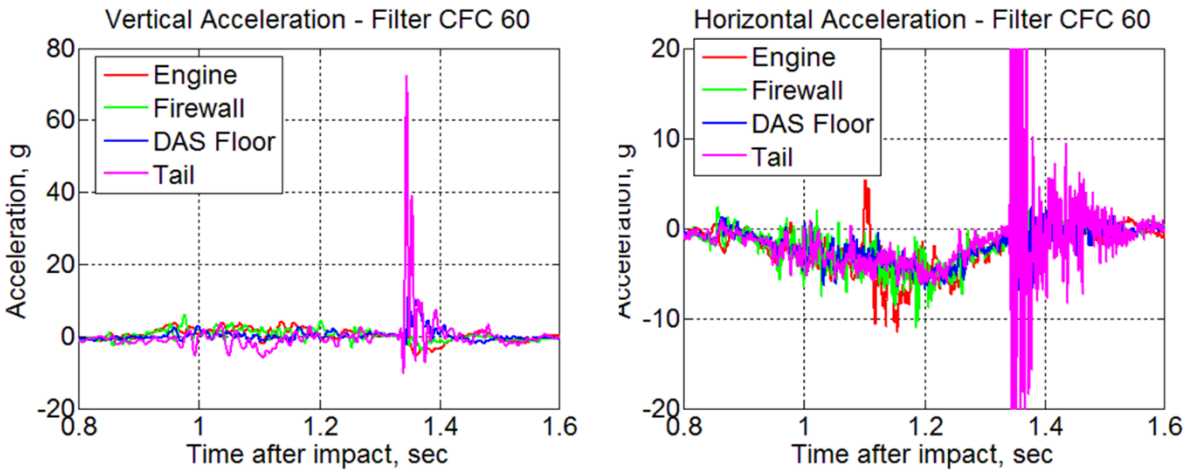

Figure 11 – Test 1 airframe accelerations during net contact

A complete summary of accelerations from Test 1 is presented in Appendix A.

The airplane, stopped by the catch net, came to rest approximately 50 feet away from the initial impact location. The net was wrapped around the nose and wings of the airplane, stopping it within 20 feet of first contact. A photograph showing the post-test airplane and net is shown in Figure 12.

Figure 12 - Airplane configuration post-test

One of the first things that was noticed during post-test inspection was the unusual orientation of the nose gear. The gear, while still intact, exhibited an unusual forward lean angle, pointing much further forward than before the test. Inspection of the high speed videos suggests that the firewall attachment location of the gear buckled under the loads seen from the initial ground contact and the compression of the nose gear

during the time in which the main gear was deforming. This finding was confirmed when conducting post-test inspections of the firewall with the nose cover skin removed. The buckling of the firewall also caused dents to appear in the nose cover skin, as seen in Figure 13.

Figure 13 - Test 1 – Post-test nose buckling and landing gear orientation

Damage also occurred on the wings near the wing strut attachment locations. It was also at this approximate location where a vertical strap from the catch net was located. The tension in the net occurring from the forward airplane velocity caused the net to start to compress the wing leading edge at the vertical strap location.

It should also be noted that the main landing gear and wheel is visible in Figure 14. All post-test inspections of the main landing gear springs showed no signs of damage, even after the landing gear exhibited large amounts of deformation during the initial ground contact. One major finding was the deformation from the ground contact did not plastically deform the gear. The wheels themselves still held air post-test, and the airplane was able to be rolled away back into the preparation hangar from the impact location for tear down.

Figure 14 - Test 1 – Post-test wing damage

When examining the underside of the aircraft, the post-test inspections showed no damage on aircraft belly skin. A small portion of the vertical stabilizer broke away from the airplane during the second tail contact, which occurred during the net catch, as shown in Figure 15. Inspections of the internal structure of the tail showed small signs of buckling, mainly in the long unsupported spans where only the thin aircraft skin was present.

Figure 15 - Test 1 – Post-test tail damage

Test 2

Test 2 was conducted on July 29, 2015. Figure 16, left, shows the airplane on the ground prior to the start of pullback, and, right, at the drop height.

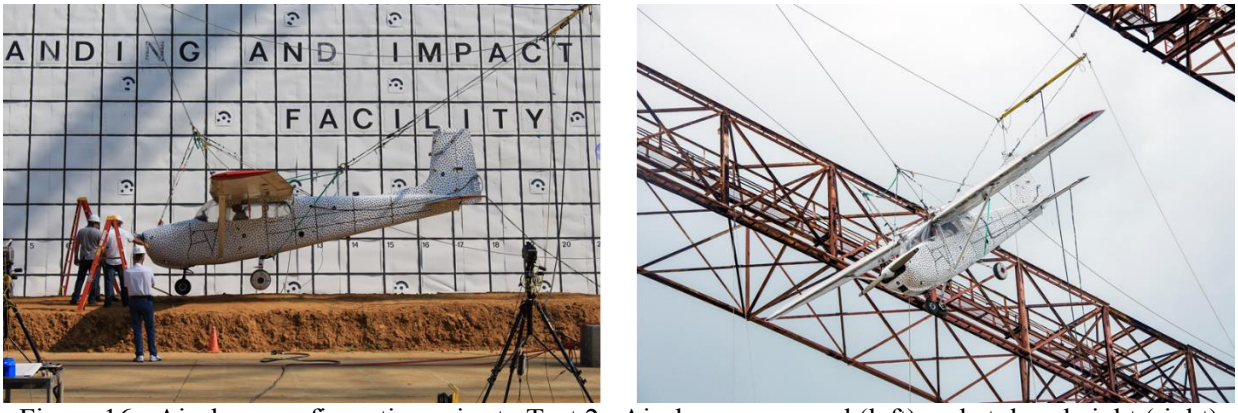

Figure 16 - Airplane configuration prior to Test 2. Airplane on ground (left) and at drop height (right)

Test 2 was the first of 2 tests where the airplane impacted a soil surface. The surface was to represent a dirt field or other type of unprepared surface not considered rigid. The airplane CG impacted the soil at a 68.6-ft/sec horizontal and 28.7-ft/sec vertical velocities. The AoA was 12.2° nose down with a pitch rate of +16.1 deg/sec.

The surface of the soil was wetted using a hose approximately one hour before the test. The moisture content for Test 2 varied between 8.8% and 22.6% by weight. Density of the soil varied between 108 lb/ft^3 and 127 lb/ft^3. The bearing capacity at one particular location is shown in Figure 17.

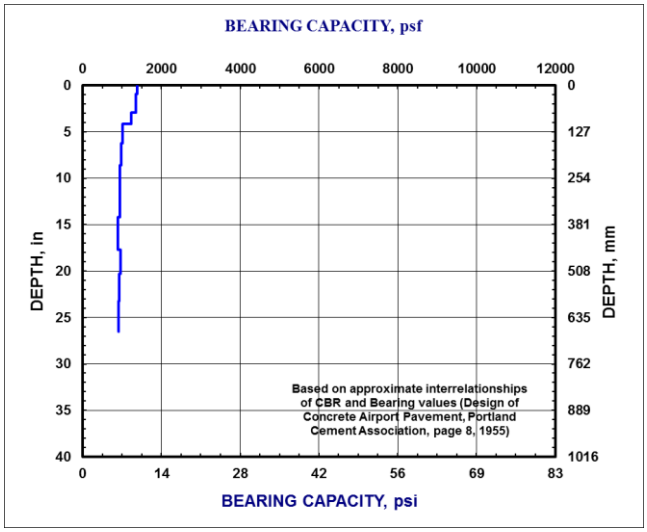

Figure 17 - Bearing capacity of the soil in Test 2

The airplane nose gear impacted the soil first and began to plow into it. The nose of the airplane impacted the soil approximately 0.070 sec after initial nose gear contact with the soil. The nose and nose gear plowing into the soil continued to occur until the left wing broke away from the fuselage at 0.111 sec after impact. At 0.169 sec after impact, the plowing caused the tail to buckle, and at 0.240 sec after impact, the airplane

started to flip over. The flipping occurred due to the penetration of the nose gear into the soil. While the soil stopped the nose gear's motion, it also created a pivot point for the rest of the airplane to rotate around. At some point during the rotation, the nose gear broke away from the rest of the airplane. This sequence is captured in Figure 18.

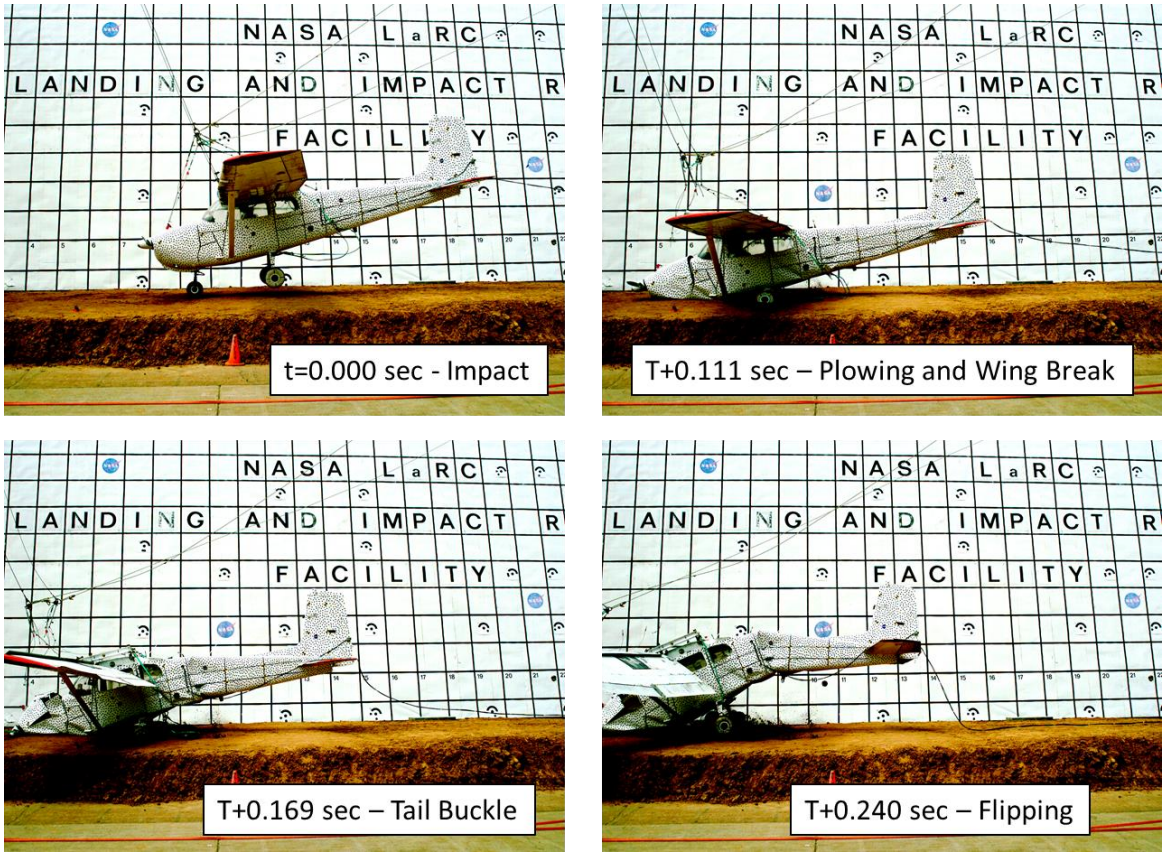

Figure 18 - Test 2 impact sequence - side view

The rest of the impact was captured from an end view camera. The rotation of the airplane continued to occur until the airplane landed upside-down approximately 1.976 sec after impact. It continued to rock back and forth until it came to final rest 6.790 sec after impact. Figure 19 shows the continuation of the impact sequence.

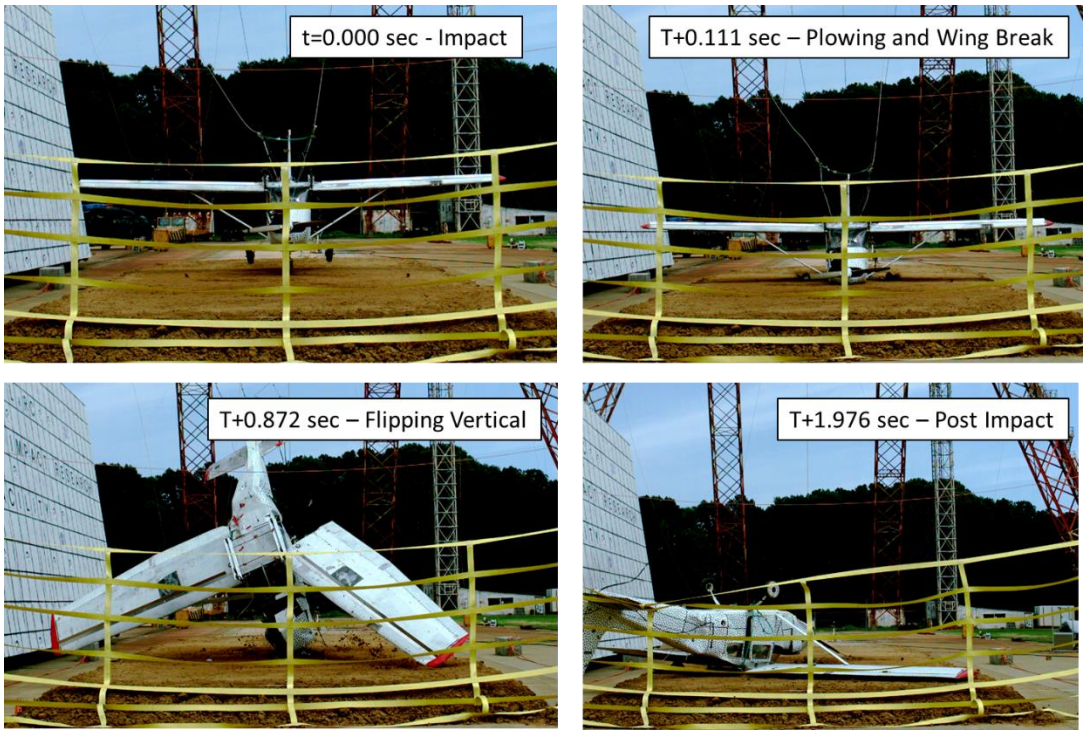

Figure 19 - Test 2 impact sequence - end view

Table 6 summarizes these events in tabular form.

Table 6 - Event timing for Test 2

Event	Time after impact (sec)
Nose gear impact	0.000
Main gear impact	0.026
Nose impact	0.071
Left Wing Break	0.111
Airplane nearly vertical	1.035
Tail net contact	1.896
Motion Stop	6.790

Vertical accelerations from the different portions of the airplane are different in magnitude, duration and shape, as shown in Figure 20. The engine experiences a peak acceleration of less than 9 g, which occurred 0.118 sec. after impact, after which, the engine experiences negative accelerations for the next 0.100 sec. The cabin of the airplane experiences maximum accelerations. The pilot floor accelerometer, located in the forward cabin, and the DAS floor accelerometer, located in the rear cabin, show peaks of 23.2 and 24.7 g, respectively. The tail acceleration starts negative, but then resembles a 0.130-sec plateau shape at +8.1 g mean acceleration.

Horizontal accelerations, shown in Figure 20, exhibit similar responses for both shape, magnitude and duration for all locations, with the exception of a large spike in the DAS floor. Engine acceleration is not plotted due to a severed cable which resulted in signal loss from that location, and the firewall location is also not plotted due to a small signal to noise ratio. The horizontal acceleration resembles a 0.135-sec triangular pulse with negative peaks of 27.1 g, 39.5 g and 19.9 g for the pilot floor, DAS floor and tail,

respectively. The average acceleration for the pulse shape is 18.7 g, 18.4 g and 13.5 g for the pilot floor, DAS floor and tail, respectively.

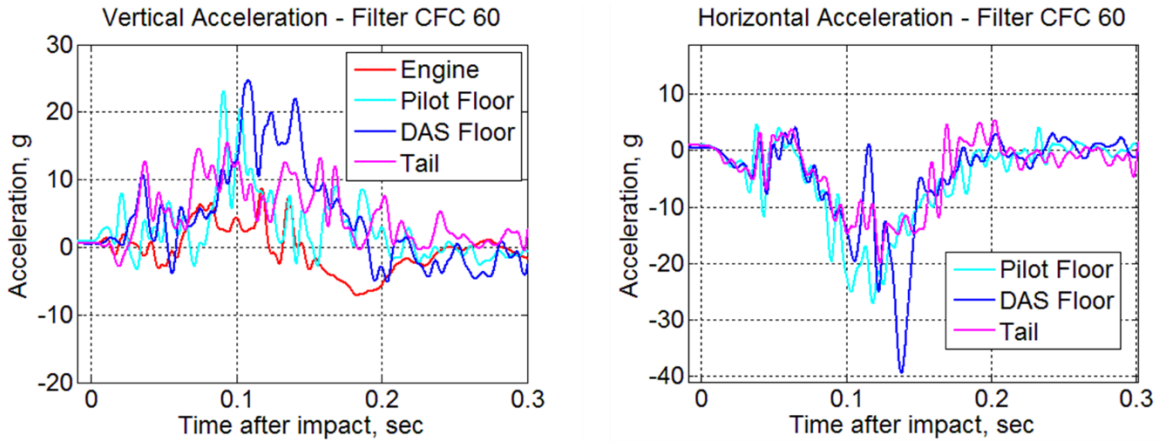

Figure 20 - Test 2 airframe accelerations

A complete summary of accelerations from Test 2 is presented in Appendix A.

The airplane came to rest on the soil surface approximately 20 feet away from the impact point, upside-down and skewed toward the co-pilot's direction. The short slide-out distance is due to the flipping of the airplane at impact. The aircraft and separated nose gear can be seen in Figure 21.

Figure 21 - Airplane configuration post-test

Major nose damage was caused by the nose gear protruding into the dirt, causing a large bending moment about the firewall. The firewall buckling caused skin damage seen in the nose of the airplane. The nose gear also broke free from the firewall and ended up in the soil, approximately 10 feet away from the airplane. The damage in the underside of the nose is shown in Figure 22. Some of this damage was caused by the firewall buckling and landing gear breaking away, while some was caused by the underside of the nose penetrating into the dirt, shearing portions of the skin near already failed regions near the firewall. The propeller, however, appeared to be intact, with only a small amount of denting on the spinner.

Figure 22 – Test 2 – Post-test nose damage

Figure 23 shows the extent of the damage on the co-pilot side of the airframe. A large gap, along with a large amount of skin buckling can be seen at the firewall location by the nose, and along the lower portion of the nose, near where the nose gear would normally be. Cabin damage is most noticeable by noting the co-pilot door has broken free from the rest of the airframe. The removed door, along with the creases in the skin behind the door, indicate large amounts of bending in the cabin area of the fuselage also.

Figure 23 – Test 2 – Post-test airframe damage - Nose and co-pilot side cabin

Damage on the pilot side of the airframe is most notable by examining the wing attachment locations, as shown in Figure 24. The attachment brackets on the wing connections fractured, causing the wing to come completely dislodged at the wing attachment locations on the fuselage and come to rest next to the body of the airplane. Further inspections of the wing attachment locations post-test suggest that age and wear on the wing attachment brackets caused this failure.

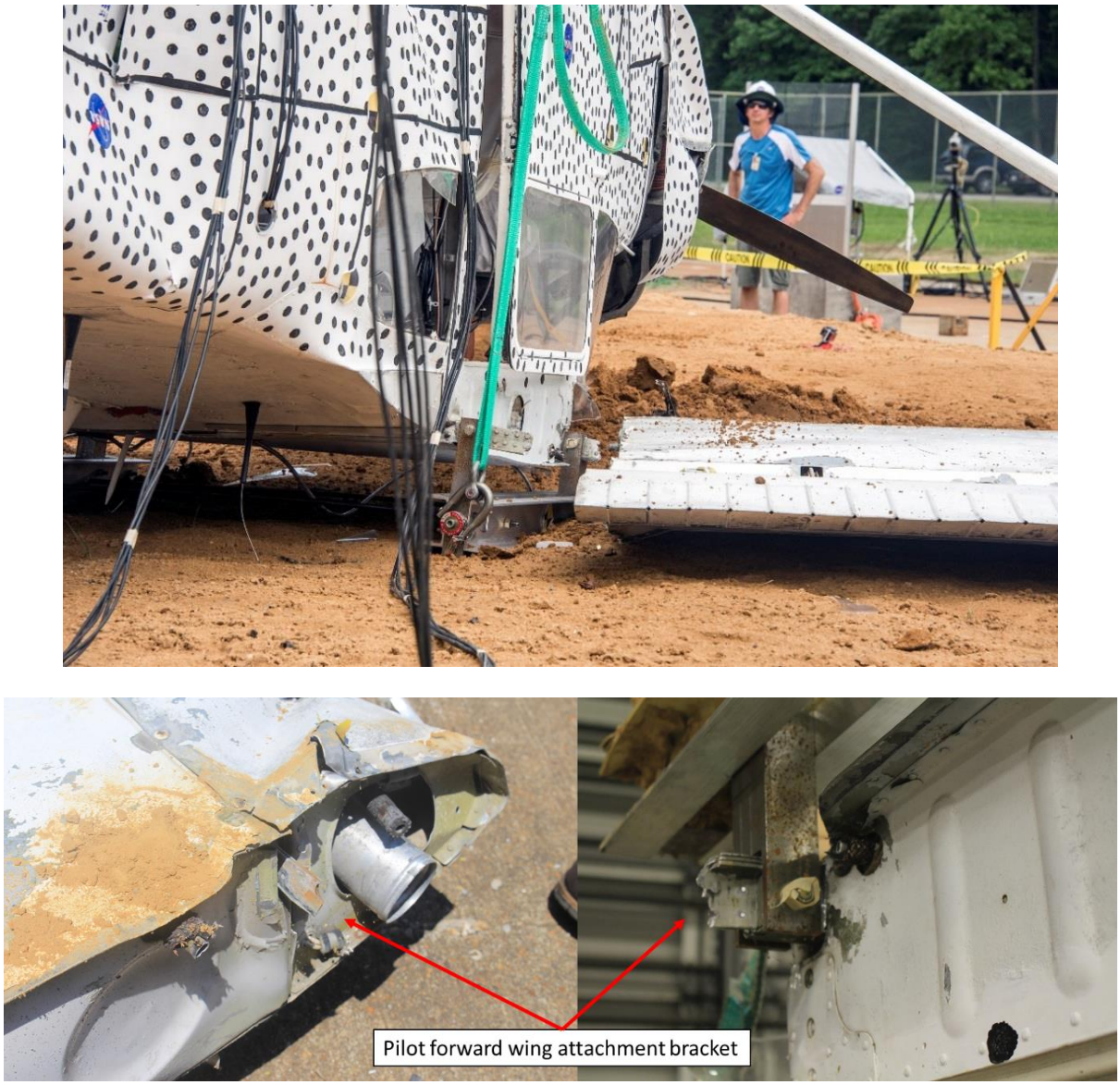

Figure 24 – Airframe damage - Pilot's wing. At impact location (top) and further inspections in the hangar (bottom)

The tail also saw a large amount of deformation during the test, however it did not break free of the cabin. Instead, large amounts of buckling were examined in the area slightly aft of station 108, as shown in Figure 25. It is at this location where the floor of the cabin ends, and thus presents an area of differing overall airframe stiffness. It is likely because of the difference in stiffness that the buckling occurred in this region.

Figure 25 – Test 2 – Post-test pilot side tail damage

Test 3

Test 3 was conducted on August 26, 2015. Figure 26 left, shows the airplane on the ground prior to the start of pullback supported in its impact condition by large blocks, and, right, at the drop height.

Figure 26 - Airplane configuration prior to Test 3. Airplane on ground (left) and at drop height (right)

Test 3 also impacted a soil surface. As with Test 2, the surface was to represent a dirt field or other type of unprepared surface not considered rigid. As shown in Figure 27, the surface was tilled on the day of the test to remove any surface compaction that may have occurred due to personnel walking on it leading up to

the test day, since the soil was left in place for 4 weeks between Tests 2 and 3. The soil was not wetted down immediately prior to the test.

Figure 27 – Preparing the soil surface prior to Test 3

The airplane CG impacted the soil at a 56.9-ft/sec horizontal and 23.6-ft/sec vertical velocities. The AoA was 8° nose up with a pitch rate of +13.3 deg/sec. There was a slight amount of roll (right side high) and yaw (nose left) to the test article for Test 3.

Due to the slight amount of roll and yaw, the airplane left main gear impacted the soil first. As the tire and the gear deformed, the tail contacted the surface at 0.030 sec after impact. The nose gear, along with the nose of the airplane contacted the surface at 0.116 sec after impact. As with Test 2, it was after the nose gear penetrated into the soil surface that the airplane started to exhibit a rotation around the nose. Unlike Test 2, however, the tail developed a fracture aft of station 108 at 0.138 sec after impact. This fracture caused the tail to peel away from the fuselage, acting much like a hinge. A small portion of skin on the bottom of the aircraft retained the tail to the rest of the airplane during the rotation. The rotation of the aircraft lasted until approximately 1.53 sec after impact, at which time the ceiling of the airplane contacted the soil. The airplane rocked for a few seconds before finally coming to rest at almost 5 sec after initial impact. A time sequence is depicted in Figure 28, as captured from one of the black and white side view cameras and Figure 29, as captured by the end view camera.

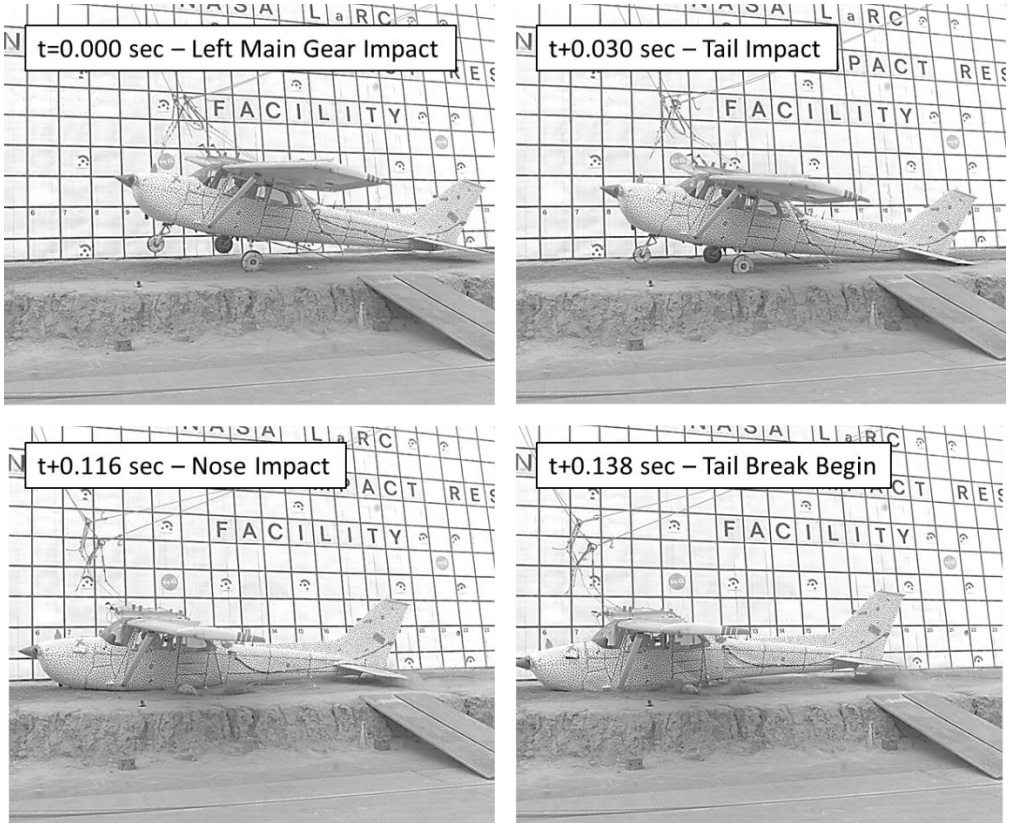

Figure 28 - Test 3 impact sequence - side view

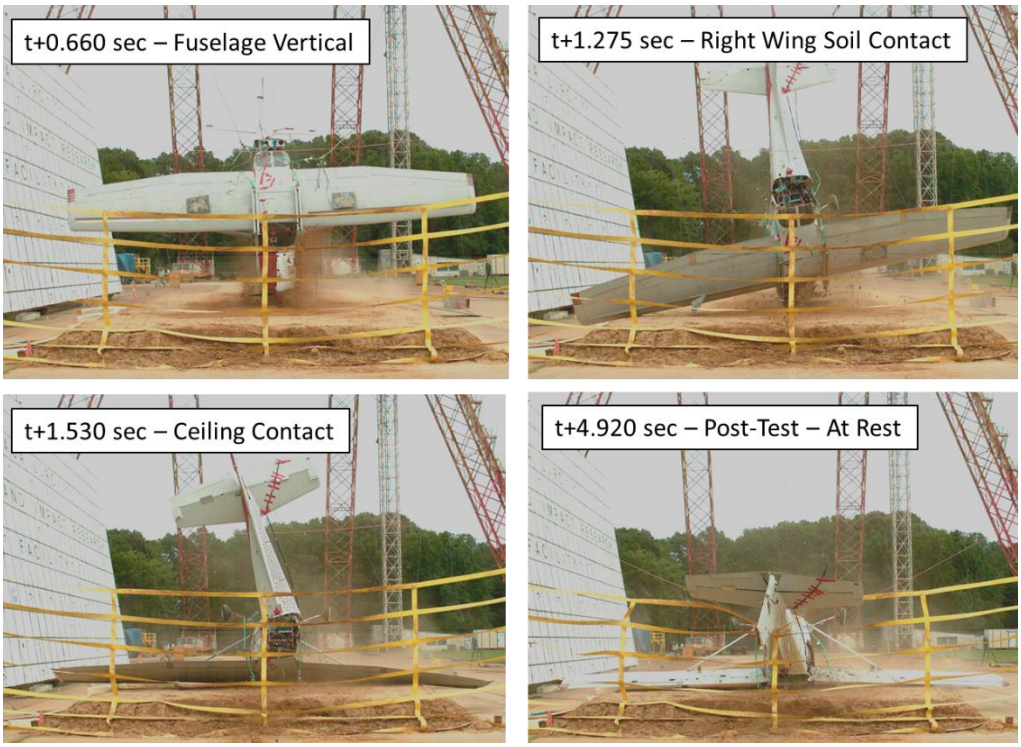

Figure 29 - Test 3 impact sequence - end view

Table 7 shows the timing sequence for Test 3.

Table 7 - Event timing for Test 3

Event	Time after impact (sec)
Left main gear contact	0.000
Tail contact	0.030
Nose contact	0.116
Tail break begin	0.138
Fuselage Vertical	0.660
Ceiling contact (upside-down)	1.530
Motion stop	4.920

Figure 30 shows the airframe accelerations. A slap down effect can be seen in the vertical acceleration plots. The tail strike is first captured by the instrumentation approximately 0.080 sec after initial impact and reaches a peak of approximately 32 g. The peak accelerations from locations going from aft to forward then occur in sequence. These accelerations reach their peaks of 27.5 g, 26.0 g, and 15.5 g, at 0.165 sec, 0.193 sec and 0.206 sec after first contact for the DAS floor, firewall and engine, respectively. The vertical acceleration pulse duration for all locations is approximately 0.240 sec.

The horizontal accelerations resemble either a triangular or trapezoidal pulse shape, depending on the location under investigation. The engine acceleration peaks at -22.1 g at 0.210 sec after impact, shaped over a 0.180-sec triangular pulse. The firewall, exhibited a peak acceleration of -38.9 g; however, this peak is likely due to the increased noise in the signal from the firewall location. The peak occurs at 0.165 sec after impact and the shape also resembles a 0.180-sec triangular pulse. The DAS floor and tail are more representative of a trapezoidal pulse, having a 0.050-sec sustained acceleration and a total pulse width of 0.250 sec. The DAS floor sustained peak acceleration is approximately -8.7 g, while the tail reaches a sustained peak acceleration of -8.1 g. The accelerations are caused from the dragging of the airplane through the dirt before rotation around the nose gear tire begins, and they occur mainly in the rear portions of the airplane due to the tail strike condition.

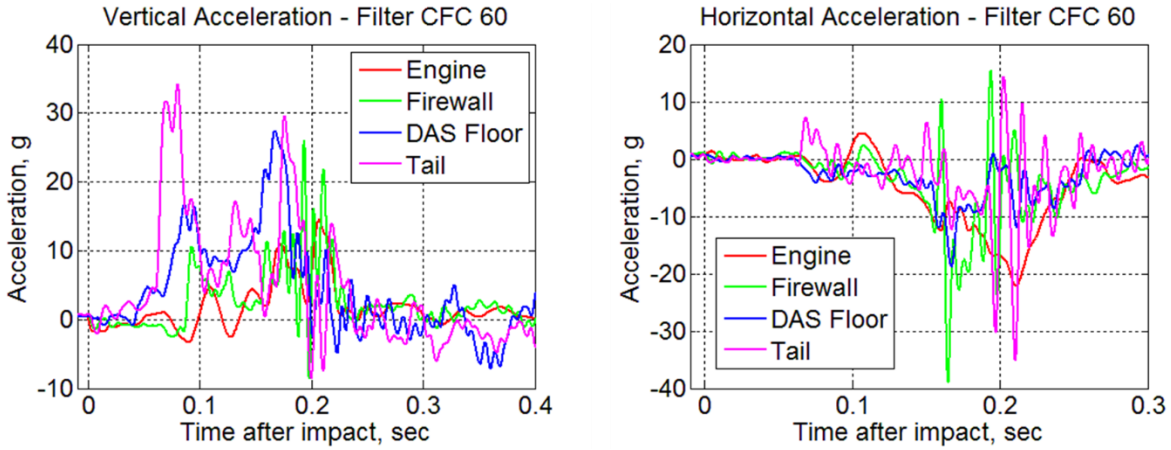

Figure 30 - Test 3 airframe accelerations

A complete summary of accelerations from Test 3 is presented in Appendix A.

The moisture content for Test 3 varied between 11% and 14% by weight. Density of the soil varied between 138 lb/ft^3 and 152 lb/ft^3. The bearing strength of the soil at the surface was about 1300 lb/ft^3, which dropped

to approximately 800 lb/ft^3 at a depth of 1 foot, and sustained this strength to the bottom depth of 2 feet. The bearing capacity as a function of depth is shown in Figure 31.

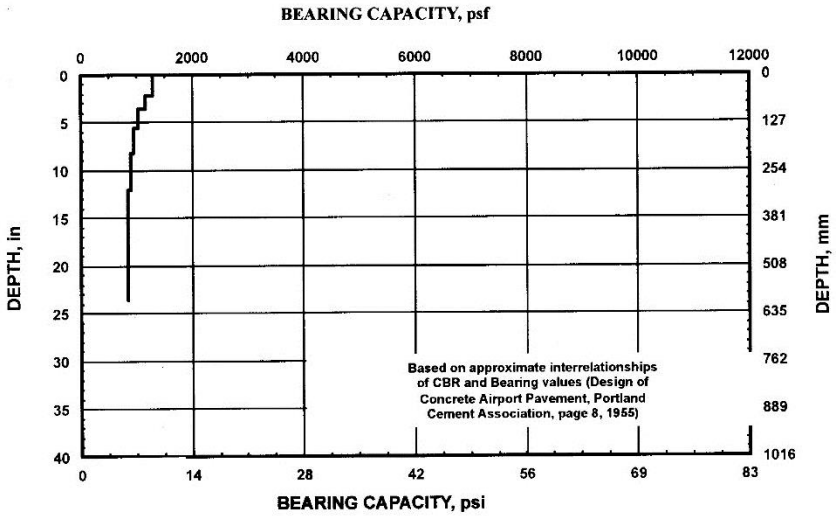

Figure 31 - Bearing capacity of the soil for Test 3

The airplane came to rest on the soil surface approximately 20 feet away from the impact point, upside-down and slightly skewed toward the co-pilot's direction (right side). The short slide-out distance is due to the flipping of the airplane at impact, as shown in Figure 32.

Figure 32 - Airplane configuration post-test

The nose of the airplane was much more intact than on the Test 2 airplane. Due to the slap down effect, the tail strike caused the airplane to lose much of its initial horizontal velocity, such that when the nose impacted, there was less of a shearing effect and more vertical crushing. The nose gear remained attached to the firewall, however there was still firewall damage, causing nose skin wrinkling and buckling, as depicted in Figure 33.

Figure 33 – Test 3 – Post-test nose damage

Unlike Tests 1 and 2, the landing gear on Test 3 consisted of a hollow tube design. Normally covered by fairings (removed for the crash tests), the tubular landing gear exhibited large amounts of plastic deformation post-test; however, the tubes did not break. The impact with the soil surface due to the slap-down caused these permanent deformations to occur. The wheels appeared to be intact post-test, as shown in Figure 34.

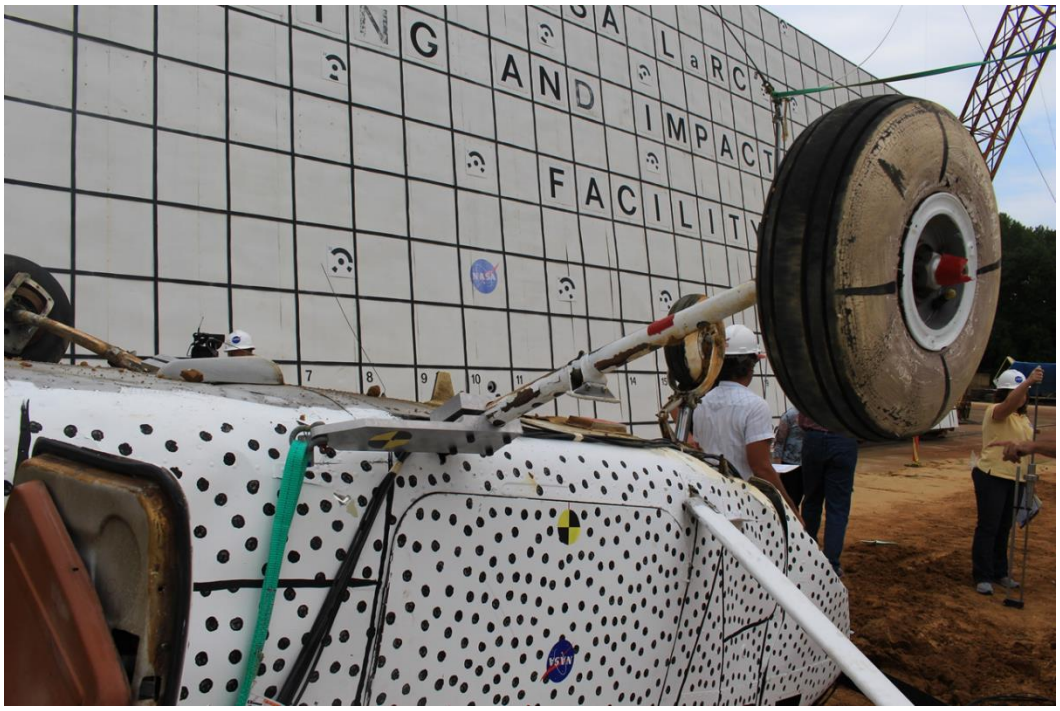

Figure 34 – Test 3 – Post-test landing gear deformation

The tail fracture occurred just aft of the 108 station in the airplane, where the cabin transitioned into the tail. This transition area offered an ideal place for failure due to the differences in stiffness. A still image is captured during the test in Figure 35, left, showing the opening caused by the fracture in the tail during the test. Figure 35, right, shows a close up of the fracture, which is located just aft of the rear window, at station 108.


Figure 35 – Test 3 – Post-test tail failure

Discussion

The airplane used in Test 1 sustained minor damage from the test. The major finding was the main gear springs absorbed the vertical impact velocity without showing signs of permanent damage. The main gears were fabricated from single pieces of 0.7-in. thick spring steel and hinge attached to the airframe at locations under the cabin floor. It is due to the bending of the main gear that the vertical acceleration was sustained for such a long time and at a relatively low (compared to the other two tests) level. The addition of the

catch net proved to be beneficial in simulating an impact into a berm or brush, due to the onset rate, peak and duration of the horizontal acceleration. It is from the catch net that the wings saw their damage. The belly of the aircraft was undamaged during the test, with only the tail striking the rigid surface during both the initial ground contact, and also during the net catch.

Tests 2 and 3, while different in their impact conditions, both resulted in the airplane flipping over and sustaining large amounts of damage. These similar results are due to the nose gear contacting and penetrating the dirt surface, causing a large rotation around the front of the airplane. Also, once the main gear penetrated the dirt, the horizontal velocity pushes the fuselage of the aircraft around the nose, resulting in large amounts of damage near the firewall area. In the case of Test 2, the nose gear attachment sheared completely off during the crush of the nose from the dirt and the flipping of the aircraft.

Test 3 was the only test that impacted in a tail strike configuration. It is from this tail strike configuration that the airframe exhibited a slap down effect. A slap down is where the tail strike caused a rotation in the cabin section about the tail resulting in higher vertical acceleration in the forward portions of the aircraft. However, the slap down effect only occurred until the nose gear penetrated the soil. After the nose gear penetrated the soil, the aircraft from Test 3 mimicked the result from Test 2 by flipping over and landing upside-down.

In both of the tests conducted onto soil, the tail buckled just aft of the cabin-tail junction. Even with the differences in tail design (straight tail for Test 2 and swept tail for Test 3), the difference in global stiffness between the cabin and tail resulted in an ideal spot for the initiation and propagation of buckling. The difference, however is the straight tail only showed signs of major buckling whereas the swept tail did exhibit fracture. The addition of the rear window in the swept tail design likely weakened the tail structure enough to cause the fracture, along with the differences in impact conditions, made for a larger vertical acceleration in the tail for Test 3.

Differences in the landing gear seemed to have little effect on the overall aircraft response for the tests conducted on soil. Test 2 main gear was the same spring steel design as Test 1, while the Test 3 gear were fabricated from a hollow tube. The difference in the performance, however, was negligible from the main gear, as the overall response was mainly dominated by the nose gear/soil interaction. Test 3 landing gear, however, was the only gear that exhibited permanent deformation when examined post-test.

In all three tests, the available volume in the cabin remained intact enough as to not infringe into the onboard occupants. The restraints used on each test were different for both the pilot and co-pilot, and while different, all of the restraints used kept both occupants strapped into their seats post-test for all three tests, even while the airplanes were orientated upside-down. Various criteria and metrics for the determination of occupant injury will be applied on the occupant and restraint data at a future time.

Conclusions

Three crash tests were successfully conducted on three Cessna 172 GA aircraft at NASA LaRC's LandIR facility during the summer of 2015. These tests served to generate data for three differing crash conditions in order to assess ELT performance. Airframe, ATD and ELT acceleration data, as well as high speed video data showing airframe deformation and ELT survivability were all generated from the crash test series. Results from airframe acceleration and general deformation data are presented in this report. Future reports will discuss ELT peroformance, occupant survivability, and photogrammetry results.

These test data will be also used in computer modeling efforts to ensure that created computer models of the three tests are within calibration parameters. Once calibration is complete, these computer models can

be used to simulate a potential infinite number of crash conditions not tested in this test series to further understand loading conditions which occur in a wide range of crash types.

The data will also be used to guide the develepment for next generation ELT guidelines, by providing insight as to the response of ELTs under three realistic crash conditions. The results can also be used as a basis for comparisons for certain types of real airplane crashes, and may help guide post-crash investigations. Finally, due to the extensive video coverage used in each test, the precise sequence of events can be scrutinized, which can lead to increased understanding of what happens during real GA airplane crashes, which will ultimately be used to save lives in the aviation community.

Acknowledgements

This research was funded by NASA Search and Rescue (SAR) Mission Office located at Goddard Space Flight Center in Greenbelt, MD. Thanks to all SAR management for their support and all of the engineers and technicians at the NASA LandIR facility for working with the utmost competence and efficiency to achieve three successful tests in such a short timeframe.

References

[1] Jackson, K.E. et al. "A History of Full-Scale Aircraft and Rotorcraft Crash Testing and Simulation at NASA Langley Research Center." NASA TM-2004-0191337. January 2004.

[2] Federal Aviation Administration. "Dynamic Test of Part 23 Airplane Seat/Restraint Systems and Occupant Protection." FAA AC 23.562-1. June 22, 1989.

[3] Carden, H.D. "Full-Scale Crash-Test Evaluation of Two Load-limiting Subfloors for General Aviation Airframes." NASA TP-2380. December 1984.

[4] Carden, H.D. "Evaluation of Emergency Locator Transmitter Performance in Real and Simulated Crash Tests." NASA TM-81960. 1981.

[5] Thomson, Robert G., and Robert C. Goetz. "NASA/FAA General Aviation Crash Program – A Status Report." J. Aircraft Vol. 17, No. 8. PP. 584-590. August 1980.

[6] Castle, C.B and Emilio Alfaro-Bou. "Crash Tests of Three Identical Low-Wing Single-Engine Airplanes." NASA TP-2190. September 1983.

[7] Castle, C.B and Emilio Alfaro-Bou. "Light Airplane Crash Tests at Three Flight-Path Angles." NASA TP-1210. June 1978.

[8] Alfaro-Bou, E., and Victor L. Vaughan, Jr. "Light Airplane Crash Tests at Impact Velocities of 13 and 27 m/sec." NASA TP-1042. November 1977.

[9] Castle, C.B and Emilio Alfaro-Bou. "Light Airplane Crash Tests at Three Roll Angles." NASA TP-1477. October 1979.

[10] Vaughan, V.L. and Robert J. Hayduk. "Crash Tests of Four Identical High-Wing Single-Engine Airplanes." NASA TP-1699. August 1980.

[11] NASA. "NASA's Gantry: Past, Present and Future Asset to Exploration." http://www.nasa.gov/centers/langley/news/factsheets/fs-2007-08-138-larc.html. Accessed September 10, 2015.

[12] NASA. "Hydro Impact Basin." http://www.nasa.gov/centers/langley/exploration/hib.html. Accessed August 17, 2015.

[13] Vaughan, V.L. and Emilio Alfaro-Bou. "Impact Dynamics Research Facility for Full-Scale Aircraft Crash Testing." NASA TN-8179. April 1976.

[14] Society of Automotive Engineers. "Surface Vehicle Recommended Practice: Instrumentation for Impact Test-Part 1- Electronic Instrumentation." SAE J211-1, July 2007.

[15] Annett, M.S., et al. "Evaluation of the First Transport Rotorcraft Airframe Crash Testbed (TRACT 1) Full-Scale Crash Test." NASA TM-2014-218543. October 2014.

[16] Thomas, M.A et al. "Constitutive Soil Properties for Unwashed Sand and Kennedy Space Center," NASA CR-2008-215334. July 2008.

APPENDIX A

ACCELERATION DATA SUMMARY

Acceleration data presented in the below tables represents a summary of the data collected from the tests. The columns presented are as follows: average acceleration, peak acceleration, event starting time, pulse duration, and delta velocity (delta-v).

The average acceleration was determined from taking the mean value of the acceleration curves starting at the start of the acceleration event (event start) and lasting through the pulse duration. This number differs from the average peak acceleration reported in the above sections. An average peak acceration reported in the above sections represents a smoothed (typically a point averaged) peak acceleration value.

The peak acceleration was extracted from the maximum value on the filtered acceleration curve between the event start and pulse duration. Note that the post-test data filtering type and value greatly affects this number. Caution must be used when only reporting this number, as it should be reported in conjunction with the average, or averaged peak, described above.

Event start and event duration indicate the beginning of the decelerations due to the impact event. The event starting point was the time in the data trace that showed a non-zero significant deceleration, and the event duration lasted through the impact event. The pulse duration for each test was identical for all sensors for each test, however the pulse durations between tests were different due to the differing impact conditions.

Delta velocity values represent an integrated value arising from the integration between the start of the event and lasting through the pulse duration, and is reported in terms of feet per second.

For cells labeled N/A, data are not available.

Table A.1 – Test 1 Acceleration Data Summary										
	Horizontal – *Reported for Catch Net Capture*					Vertical – *Reported for Ground Impact*				
	Average Acceleration (+g)	Peak acceleration (+g)	Event Start (sec)	Event Duration (sec)	Delta-v (fps)	Average Acceleration (g)	Peak Acceleration (g)	Event Start (sec)	Duration (sec)	Delta-v (fps)
Engine	3.3	11.5	0.8629	0.500	53.4	4.1	12.3	0.015	0.185	24.4
Firewall	3.0	16.7	0.8629	0.500	48.5	4.3	11.4	0.015	0.185	25.7
Forward cabin	2.9	29.8	0.8629	0.500	46.9	4.8	10.4	0.015	0.185	28.4
Left Door Frame	3.1	27.8	0.8629	0.500	52.0	4.8	14.0	0.015	0.185	28.7
Right Door Frame	2.8	19.8	0.8629	0.500	45.7	4.8	13.3	0.015	0.185	28.2
Rear Cabin (DAS)	2.8	9.9	0.8629	0.500	44.9	4.6	15.3	0.015	0.185	30.0
Tail	4.0	23.7	0.8629	0.500	48.9	5.9	54.7	0.015	0.185	35.0

Table A.2 – Test 2 Acceleration Data Summary										
	Horizontal					Vertical				
	Average Acceleration (+g)	Peak acceleration (+g)	Event Start (sec)	Duration (sec)	Delta-v (fps)	Average Acceleration (g)	Peak Acceleration (g)	Event Start (sec)	Duration (sec)	Delta-v (fps)
Engine	N/A	N/A	N/A	N/A	N/A	2.3	8.7	0.036	0.164	7.8
Firewall	N/A	N/A	N/A	N/A	N/A	N/A	N/A	N/A	N/A	N/A
Forward cabin	18.7	27.1	0.065	0.135	48.5	7.0	23.2	0.036	0.164	27.9
Left Door Frame	14.1	24.5	0.065	0.135	38.9	13.1	29.7	0.036	0.164	30.7
Right Door Frame	16.3	24.0	0.065	0.135	44.8	14..3	35.6	0.036	0.164	36.9
Rear Cabin (DAS)	18.4	39.5	0.065	0.135	42.9	17.4	24.7	0.036	0.164	46.3
Tail	13.5	19.9	0.065	0.135	33.5	8.1	15.5	0.036	0.164	39.5

Table A.3 – Test 3 Acceleration Data Summary										
	Horizontal					Vertical				
	Average Acceleration (+g)	Peak acceleration (+g)	Event Start (sec)	Duration (sec)	Delta-v (fps)	Average Acceleration (g)	Peak Acceleration (g)	Event Start (sec)	Duration (sec)	Delta-v (fps)
Engine	5.9	22.1	0.0575	0.323	50.2	2.5	15.5	0.010	0.239	18.3
Firewall	4.5	38.9	0.0575	0.323	38.6	3.7	26.0	0.010	0.239	27.1
Forward cabin	5.3	18.1	0.0575	0.323	45.7	5.0	18.0	0.010	0.239	38.5
Left Door Frame	4.3	16.1	0.0575	0.323	41.2	6.7	20.2	0.010	0.239	50.0
Right Door Frame	N/A	N/A	N/A	N/A	N/A	6.9	18.8	0.010	0.239	50.7
Rear Cabin (DAS)	3.3	18.7	0.0575	0.323	30.5	7.9	27.5	0.010	0.239	58.2
Tail	2.4	35.2	0.0575	0.323	22.7	9.6	32.2	0.010	0.239	71.1

REPORT DOCUMENTATION PAGE

Form Approved
OMB No. 0704-0188

1. REPORT DATE *(DD-MM-YYYY)*	2. REPORT TYPE	3. DATES COVERED *(From - To)*
01- 11 - 2015	Technical Memorandum	

4. TITLE AND SUBTITLE

Crash Tests of Three Cessna 172 Aircraft at NASA Langley Research Center's Landing and Impact Research Facility

5a. CONTRACT NUMBER

5b. GRANT NUMBER

5c. PROGRAM ELEMENT NUMBER

6. AUTHOR(S)

Littell, Justin D.

5d. PROJECT NUMBER

5e. TASK NUMBER

5f. WORK UNIT NUMBER

736466.01.08.07.55.01

7. PERFORMING ORGANIZATION NAME(S) AND ADDRESS(ES)

NASA Langley Research Center
Hampton, VA 23681-2199

8. PERFORMING ORGANIZATION REPORT NUMBER

L-20622

9. SPONSORING/MONITORING AGENCY NAME(S) AND ADDRESS(ES)

National Aeronautics and Space Administration
Washington, DC 20546-0001

10. SPONSOR/MONITOR'S ACRONYM(S)

NASA

11. SPONSOR/MONITOR'S REPORT NUMBER(S)

NASA-TM-2015-218987

12. DISTRIBUTION/AVAILABILITY STATEMENT

Unclassified - Unlimited
Subject Category 39
Availability: NASA STI Program (757) 864-9658

13. SUPPLEMENTARY NOTES

14. ABSTRACT

During the summer of 2015, three Cessna 172 aircraft were crash tested at the Landing and Impact Research Facility (LandIR) at NASA Langley Research Center (LaRC). The three tests simulated three different crash scenarios. The first simulated a flare-to-stall emergency or hard landing onto a rigid surface such as a road or runway, the second simulated a controlled flight into terrain with a nose down pitch on the aircraft, and the third simulated a controlled flight into terrain with an attempt to unsuccessfully recover the aircraft immediately prior to impact, resulting in a tail strike condition. An on-board data acquisition system captured 64 channels of airframe acceleration, along with acceleration and load in two onboard Hybrid II 50th percentile Anthropomorphic Test Devices, representing the pilot and co-pilot. Each test contained different airframe loading conditions and results show large differences in airframe performance. This paper presents test methods used to conduct the crash tests and will summarize the airframe results from the test series.

15. SUBJECT TERMS

Airplane testing; Emergency locator transmitter; Full scale crash testing; Impact testing; Safety

16. SECURITY CLASSIFICATION OF:			17. LIMITATION OF ABSTRACT	18. NUMBER OF PAGES	19a. NAME OF RESPONSIBLE PERSON
a. REPORT	b. ABSTRACT	c. THIS PAGE			STI Help Desk (email: help@sti.nasa.gov)
					19b. TELEPHONE NUMBER *(Include area code)*
U	U	U	UU	39	(757) 864-9658